Cell Reports
Physical Science

CellPress
OPEN ACCESS

Report

Pulsed laser ejection of single-crystalline III-V solar cells from GaAs substrates

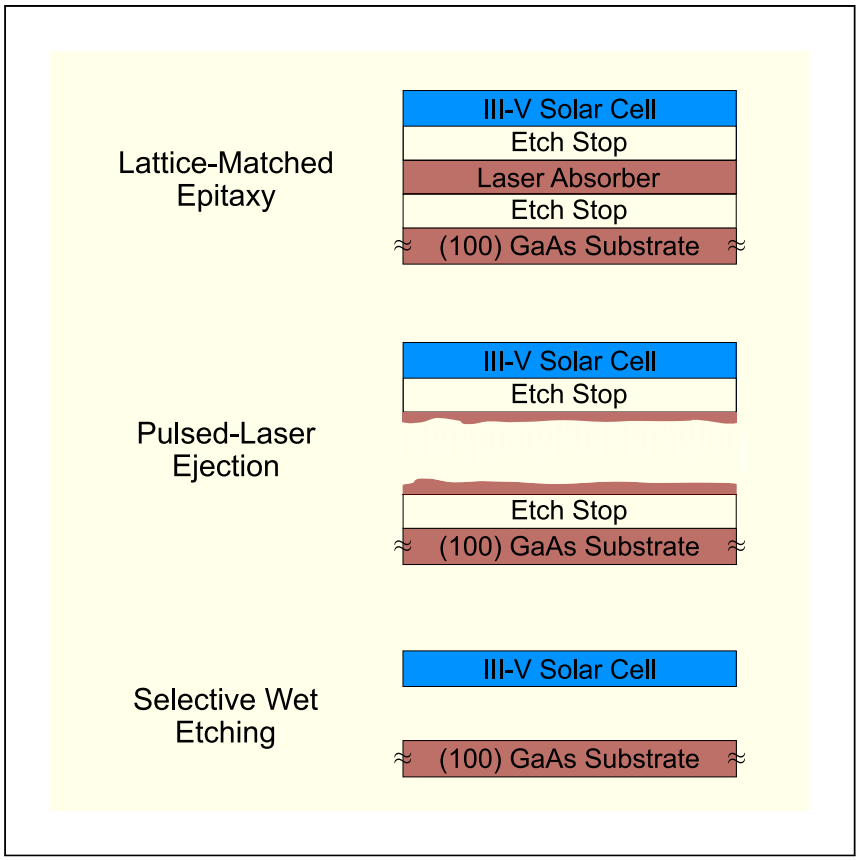

The best solar cells use single crystal, III-V active layers that are grown on GaAs wafers. Reeves et al. pop off a μm-thin, III–V multilayer from a GaAs wafer with a laser pulse, then use fast surface-processing operations to turn the crystalline thin film into a high-performing photovoltaic device.

Benjamin A. Reeves, Myles A. Steiner, Thomas E. Carver, Ze Zhang, Aaron M. Lindenberg, Bruce M. Clemens

bmc@stanford.edu

Highlights

Thin, single-crystalline III-V solar cells are removed from GaAs substrates

A laser pulse ejects a lattice-matched III-V multilayer from the GaAs wafer

High-performing solar cells are ejected and finished in minutes

Lattice-matched optical selectivity provides diverse, scalable processing paths

Reeves et al., Cell Reports Physical Science 4, 101449
June 21, 2023 © 2023
https://doi.org/10.1016/j.xcrp.2023.101449

Cell Reports
Physical Science

CellPress
OPEN ACCESS

Report

Pulsed laser ejection of single-crystalline III-V solar cells from GaAs substrates

Benjamin A. Reeves,[1] Myles A. Steiner,[2] Thomas E. Carver,[3] Ze Zhang,[4] Aaron M. Lindenberg,[1,5] and Bruce M. Clemens[1,6,*]

SUMMARY

The best III-V solar cells start out as single-crystalline multilayers on GaAs substrates. Separating these multilayers from their growth substrate enables higher performance and wafer reuse, which are both critical for terrestrial III-V solar cell viability. Here, we remove rigidly bonded, 16 mm^2 × 3.5 μm thick devices from a GaAs substrate using an unfocused Nd:YAG laser pulse. The pulse is absorbed by a low-band-gap, lattice-matched layer below the device, driving an ablation event that ejected the crystalline multilayer from the substrate. Minutes of selective wet-chemical etching and device finishing yield a 0.1 cm^2 device with a 17.4% power conversion efficiency and open-circuit voltage of 1.07 V, using AM1.5 direct with no anti-reflection coating. We show that the performance is comparable to similar cells produced via conventional processes. We discuss unique process characteristics, such as the potential to separate wafer-sized solar cells per laser pulse.

INTRODUCTION

Thin film transfer and wafer recovery processes are essential for manufacturing single-crystal III-V solar cells. III-V substrates are typically two to three orders of magnitude thicker than the active photovoltaic layers,[1] and III-V wafer costs are high because, for example, III-V elements and compounds are not abundant.[2] They are also toxic, carcinogenic,[3] and fragile,[4] and III-V wafer manufacturing utilizes specialized, encapsulated crystal pulling techniques for relatively small wafer diameters and with high material losses.[4,5] Yet, all record-holding solar cells are made from single-crystal III-V thin films that were grown on III-V substrates.[6–9] The proliferation of the highest-quality solar cells therefore depends, in part, on rapid and inexpensive processes that separate single-crystal thin films from III-V substrates while preserving wafer surfaces for regrowth.[10,11]

Driven in part by demand for lower-cost III-V photovoltaics, various III-V single-crystalline thin film transfer solutions have been developed, all of which utilize some combination of epitaxy, mechanical peeling, and selective chemical etching. Wet-chemical etch-rate ratios between lattice-matched alloys can exceed 10^6.[12,13] This etch selectivity is utilized to separate thin films from growth substrates, for example by laterally etching a 10–100 nm thick AlAs[14,15] or an AlInP[16] layer grown between a GaAs substrate and the device layers. The lateral etches become diffusion limited and stall unless the film is peeled away during etching and then proceed only at order 1–10 mm h^{-1}.[17] With spalling, a mechanical separation process, a tensile stressor layer on the thin film surface pulls open a lateral crack beneath the device layers.[18] Unfortunately, for (100) III-V substrates, cracks opening along a {100} plane

[1]Department of Materials Science and Engineering, Stanford University, Stanford, CA 94305, USA

[2]National Renewable Energy Laboratory, Golden, CO 80401, USA

[3]Stanford Nano Shared Facilities, Stanford University, Stanford, CA 94305, USA

[4]Department of Mechanical Engineering, Stanford University, Stanford, CA 94305, USA

[5]Stanford Institute for Materials and Energy Sciences, SLAC National Accelerator Laboratory, Menlo Park, CA 94025, USA

[6]Lead contact

*Correspondence: bmc@stanford.edu

https://doi.org/10.1016/j.xcrp.2023.101449

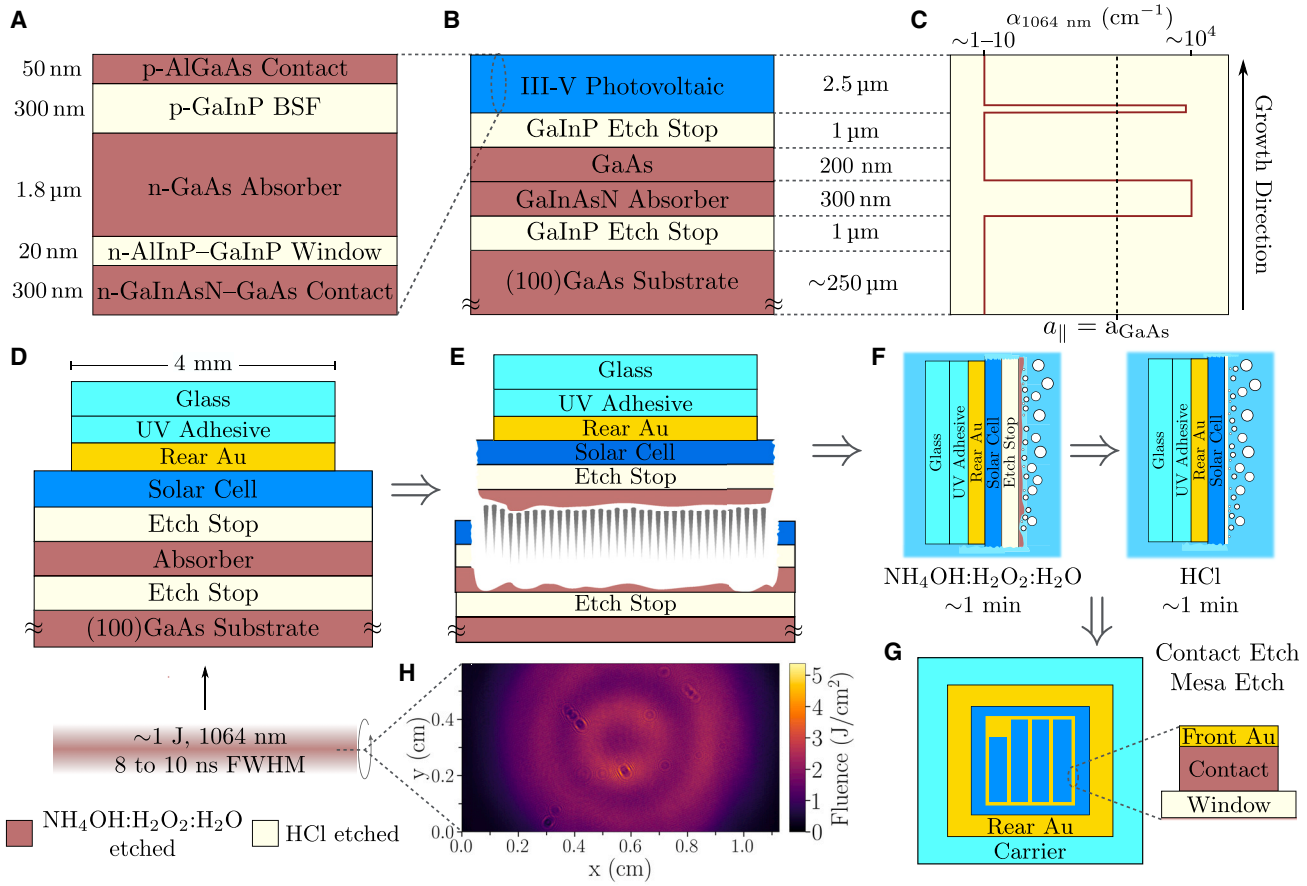

Figure 1. Overview of device fabrication with pulsed-laser crystal ejection

(A) This work used GaAs-based, single-heterojunction, inverted, lattice-matched, III-V photovoltaics.

(B) The photovoltaic was synthesized in line with the layers used for device ejection and finishing (a lattice-matched, GaInP-GaInAsN-GaAs-GaInP multilayer).

(C) The relatively narrow, direct electronic band gap of the GaInAsN absorber created a sharp absorption gradient for a Nd:YAG laser pulse inside of the crystal.

(D) After depositing an Au|Ti contact layer onto the p-AlGaAs, the Ti (not shown) was bonded to glass, and the surrounding metal etched away. The specimen was then positioned into the path of a normally incident Nd:YAG laser pulse.

(E) The laser pulse drove an ablation event inside of the crystal, which caused the photovoltaic device structure to eject from the substrate.

(F) After ejection, the melt debris and etch stop were etched away in minutes with room temperature, chemically selective etchants. Prior to etching, the glass was bonded to a larger glass carrier to improve device handling (not shown for simplicity).

(G) After electroplating the Au grid, the exposed front GaInAsN contact layer was etched down to the AlInP window. The mesa was defined with photolithography and etched, similar to (F).

(H) Our laser spatial filter could produce single- or multimode laser pulse spatial profiles. Here, we used multimode pulses to maximize transmitted energy. The small Fresnel diffraction spots rotated around the profile when rotating imaging optics and are therefore not intrinsic to the laser spatial profile.

will redirect onto the lower-energy {110} planes and potentially into device layers and the substrate.[19] Variations on spalling and chemical liftoff processes seek to address crack-confinement,[20,21] stress management,[22] lateral etching rates,[17] and surface effects.[16]

Here, we eject III-V photovoltaic devices from a GaAs wafer using a laser pulse (Figure 1) by exploiting wavelength-dependent optical absorption $\alpha(\lambda)$ differences between conventional, lattice-matched III-V layers.[23–26] Unlike previous work, we demonstrate the nearly instantaneous separation of rigidly bonded, compositionally and electronically complex thin films, as well as characteristic, rapid finishing

operations to produce high-performing devices. The device structure is a multilayer of III-V alloys, with sharp, optoelectronic property gradients, and active layers are single crystals of order 1 nm to 1 μm thick. Individual layers provide critical functionalities,[27–29] such as surface passivation with indirect, wide-band-gap III-V windows, carrier-selective transport, Ohmic contacting, and, now, additional degrees of freedom to optically split the active layers from the GaAs substrate and finish surfaces with minutes of wet etching. We compare our prototype, laser-ejected solar cells to specimens produced at the National Renewable Energy Laboratory (NREL) from mature fabrication processes and comparable metalorganic vapor phase epitaxy (MOVPE) growth parameters.

RESULTS AND DISCUSSION

Solar cell fabrication and ejection

We synthesized standard III-V thin films via MOVPE at NREL (Figures 1A, 1B, and S1; supplemental experimental procedures; Note S1). Beginning with a single-side polished (100) GaAs substrate, we grew a 1 μm thick $Ga_{0.49}In_{0.51}P$ etch stop, a 300 nm $Ga_{.93}In_{.07}As_{.98}N_{.02}$ absorber layer, a 200 nm GaAs spacing layer, and another 1 μm thick $Ga_{0.49}In_{0.51}P$ etch stop (all thicknesses and compositions are nominal). Growth continued with an inverted rear-heterojunction III-V photovoltaic cell[30] consisting of an n-$Ga_{.97}In_{.03}As_{.99}N_{.01}$ front contact layer, n-$Al_{0.52}In_{0.48}P$|$Ga_{0.49}In_{0.51}P$ window layers, an n-GaAs absorber, a p-$Ga_{0.49}In_{0.51}P$ heterojunction base, and a p-$Al_{0.3}Ga_{0.7}As$ rear contact layer. Relative to mature baseline devices, the GaInP-GaInAsN-GaAs-GaInP layer set was the only growth modification necessary for laser ejection. The two GaInAsN layers were slightly different: the laser absorber layer had ~2% N on the group V sub-lattice and ~7% In on the group III sub-lattice to lattice match the alloy, while the front contact layer had ~1% N and 3% In to lattice match. Photoluminescence and X-ray diffraction results from the $Ga_{0.93}In_{0.07}As_{0.98}N_{0.02}$ absorber layer were consistent with a pseudomorphic alloy, with a band gap of approximately 1.07 eV (Note S2; Figure S2), which is 0.1 eV less than the laser's 1.17 eV photon energy. As shown in Figure 1C, based on typical behaviors of direct-band-gap III-V alloys,[31] the GaInAsN absorber (and GaInAsN front contact) likely had absorption coefficients α(1,064 nm) of about 10^4 cm^{-1}. However, α(1,064 nm) for the other compounds were orders of magnitude lower because their electronic band gaps were greater than the photon energy, although their absorption was not zero due to the non-linear processes that occur at our order 100 MW cm^{-2} intensities.[32,33] For all layers, the lattice matching preserved the in-plane lattice parameter $a_{\parallel} = a_{GaAs}$, preventing strain-induced defects such as misfit dislocations.[34]

After MOVPE, we prepared the specimen for crystal ejection. The substrate was single-side polished for better *in situ* monitoring of the curvature and stress during MOVPE, but because the laser pulse would travel through the substrate, the substrate was polished after epitaxy to produce a specular surface and an approximate thickness of 250 μm. The specular surface was protected with photoresist until laser processing. The AlGaAs was stripped of surface oxides via wet etching, followed by e-beam evaporation of a 500 nm rear Au reflective contact, then a 40 nm Ti adhesion layer. 4 × 4 mm glass coverslips were bonded to the Ti with UV-curing adhesive and direct-write UV photolithography.

After removing the surrounding Ti and Au with wet etching, the contacted and mounted device layers were inserted normal to the optical path of a commercial, Q-switched, Nd:YAG laser, with the polished wafer surface facing the laser. The laser

produced nominally 1,064 nm wavelength, 8–10 ns full width at half maximum (FWHM) pulses (Figures 1D, 1H, and S3; Note S3). Sharp variations in the laser pulse spatial intensity profile were minimized with a vacuum-pinhole spatial filter, yielding pulses with the characteristic spatial fluence profile shown in Figure 1H, and pulse energies of about 1.1 $\pm$ 0.1 J (the small diffraction spots in Figure 1F rotated with imaging optics and are therefore imaging artifacts). After course alignment by transmission imaging of highly attenuated pulses, we removed attenuation filters and ejected the specimen (Note S3; Figure S6). We observed single-shot specimen ejection (Figure S4), but if a single pulse did not eject a specimen—due to misalignment or pulse energy fluctuation, for example—the specimen was translated by order 100 μm before firing another pulse.

The ejected specimen's glass was adhered to a glass carrier for selective wet etching and device finishing (Figures 1F and 1G). The melt debris and GaInP etch stop were removed with their respective selective etchant (the substrate could be treated analogously). We then used direct-write photolithography to develop the front contact pattern into photoresist and selectively electroplated a thin Ni adhesion layer and nominally 2 μm Au into the pattern to form the front metal grid (Figure S7). The exposed GaInAsN contact layer was removed via wet etching, and finally, a mesa was defined via photolithography and additional selective etching.

Device characterization

The device's photovoltaic performance was measured at NREL. Figure 2 shows the testing configuration, current density vs. voltage (J-V) curves under the AM1.5 direct spectrum at 1,000 W/m^2, dark J-V, and external quantum efficiency data for our best cells. We compare our laser-ejected devices with similar baseline cells grown in the same MOVPE reactor and fabricated via NREL's mature GaAs processes, where the substrate was chemically etched away.[35,36] As summarized in Table 1, our prototype-ejected devices demonstrated excellent performance metrics, near parity with the baseline. With no anti-reflection coatings, our highest performing cell showed a conversion efficiency η = (17.4 $\pm$ 0.5)%, a short circuit current density J_{sc} = (19.8 $\pm$ 0.6) mA/cm^2, an open circuit voltage V_{oc} = 1.07 V, a fill factor FF = 0.82, and a device area A = 0.105 cm^2. The external quantum efficiency data also show comparable performance, with characteristic, sharp electronic band edges, and Fabry-Perot interference fringes from the single-crystalline uniform multilayers and highly reflective back mirror. The quantum efficiency differences between the etched and ejected samples are on the order of a few percentage points at all wavelengths. The dark J-V shows a difference between the etched and ejected samples. Both sets of samples exhibit normal n = 1 diode behavior at high voltage and n = 2 behavior at low voltage, but the ejected samples show shunt-like behavior at intermediate voltages, which likely explains the reduced fill factors. The shunt-like behavior is emphasized by the log-normal plot. It would appear to be a non-linear shunt that does not affect the slope of the J-V curve (Figure 2B) near 0 V, as in a more typical shunt. Understanding and potentially mitigating this behavior was beyond the scope of this study. As discussed later, this would require lowering the total experimental uncertainty, producing larger sample sizes, and characterizing with additional techniques such as scanning electron and atomic force microscopies. Were this behavior unavoidable, it would be particularly deleterious for low-intensity applications.

We observed finished, ejected devices with bright-field, Nomarski differential interference contrast, and dark-field microscopies. Despite our inhomogeneous, multimode laser pulses (Figure 1H), we did not observe any thin film cracking or

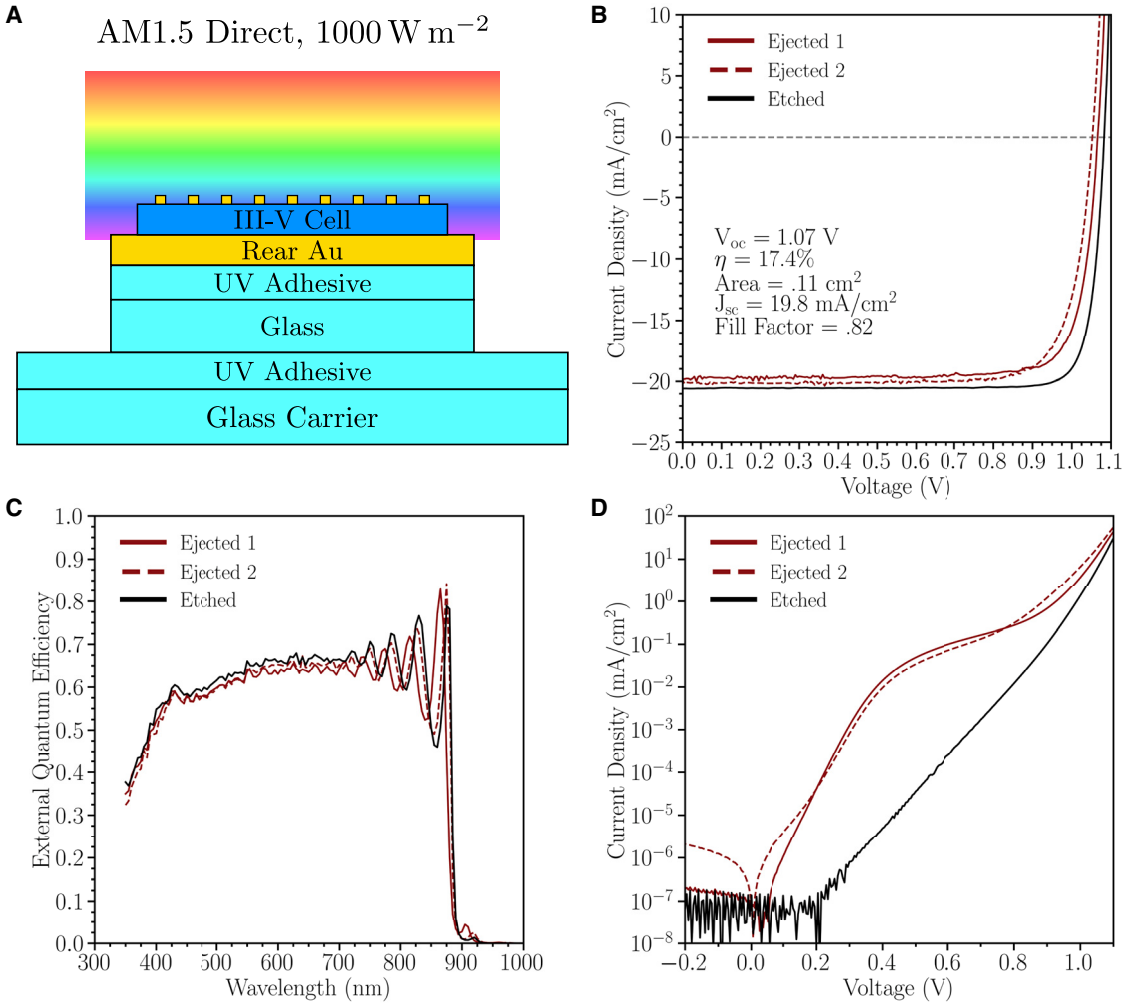

Figure 2. Results from optoelectronic device characterization

(A) J-V tests on the final ejected device structures were measured under AM1.5 direct, 1,000 W/m^2 conditions at 25°C.

(B) The ejected and etched cells showed excellent, comparable performance. The performance metrics for our best-performing ejected cell are noted in the figure and in Table 1.

(C) External quantum efficiency was comparable between etched and ejected cells.

(D) Dark curves for the ejected cells showed a non-linear shunt for the ejected devices.

other bulk damage for the device dimensions that were readily ejectable with our laser system (Figures 3A–3C and S5; Note S5). We did observe thin film damage near the ejected film edges and corners, especially after wet etching. During laser ejection, device corners were located within a few hundred microns of the sub-critical fluences near our pulse edges and could mechanically tear during ejection. Furthermore, unlike the baseline cells, our ejected devices were elevated from the

Table 1. A summary of etched and ejected device performance metrics

Device	η (%)	J_{sc} (mA/cm^2)	V_{oc} (V)	FF	Area (cm^2)
Ejected 1	17.4	19.8	1.07	0.821	0.105 (measured)
Ejected 2	17.0	19.9	1.05	0.810	0.101 (measured)
Etched	19.2	20.6	1.08	0.863	0.1005 (nominal)

Photovoltaic performance metrics for the two laser-ejected cells, and the baseline cell whose substrate was etched away with NH_4OH:H_2O_2.

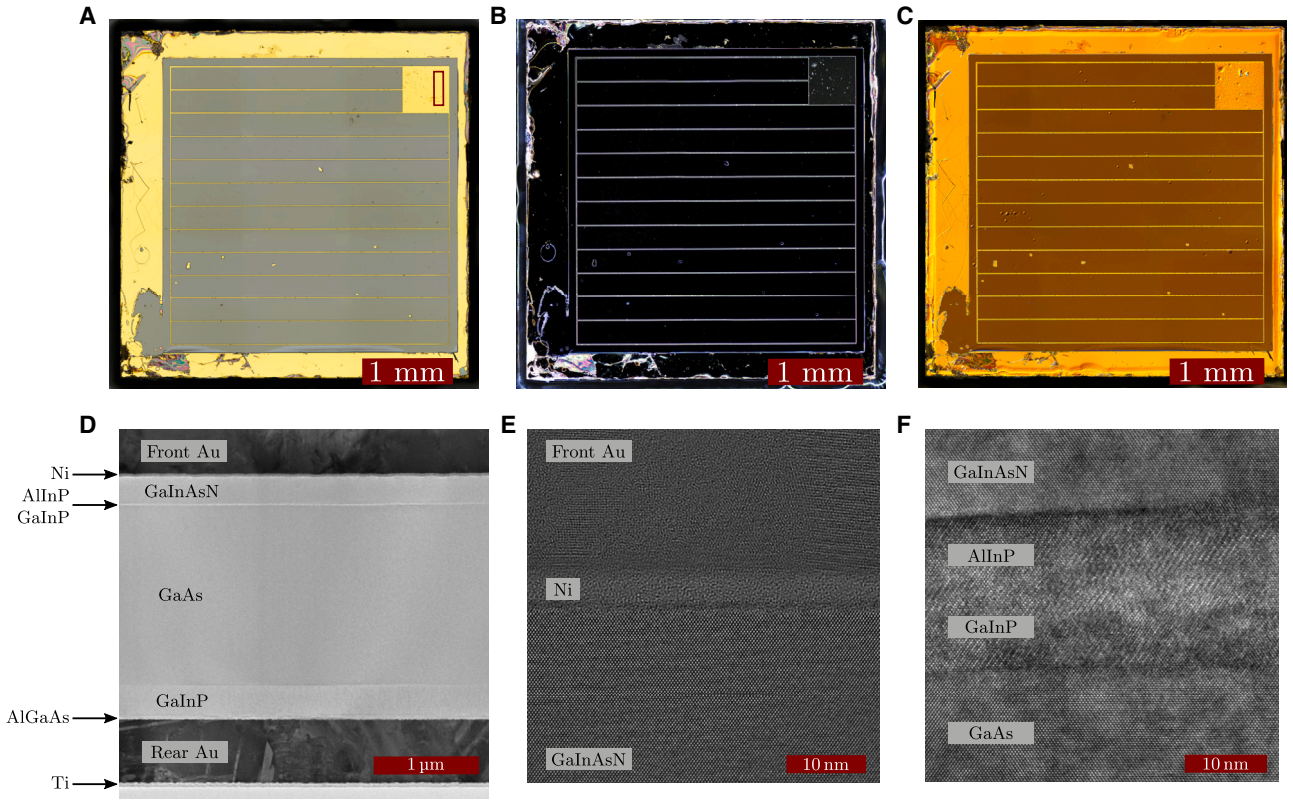

Figure 3. Optical and TEM device characterization

(A) A bright-field optical micrograph of the finished cell. The rectangle over the front contact pad shows the characteristic ion-milling location for TEM specimens. Image stitching artifacts are seen in (A)–(C).

(B) Dark-field optical microscopy reveals a crack-free surface, as well as debris on the AlInP window.

(C) Differential interference contrast microscopy also shows a crack-free surface, as well as electroplating roughness and rounded subsurface features not seen in (A) or (B).

(D) A TEM cross-section of an ejected cell, showing layer thicknesses and excellent material quality. The <100> direction is vertical, and <110> is normal to the page.

(E and F) We found no evidence of misfit dislocations or melted interfaces while searching the lamella shown in (D). The scale bars in (E) and (F) were calibrated by assuming GaAs atomic spacing in the micrographs.

surface of the glass carrier (by the Ti-bonded glass). Hence, effects such as photoresist beading and adhesive swelling along the elevated edges complicated wet etching, photolithography, and electroplating. Larger sample sizes and statistical analyses were beyond the scope of the present study. Both will be required to optimize device performance, as well as to understand any damage mechanisms, their effects, and appropriate mitigation strategies from within the vast process parameter space. Our ~1 J pulse contained enough energy to eject ~1 cm^2. However, as shown in Figure 1H (and discussed in Note S3), our fluence reached about 3–4 times higher than ~1 J/cm^2 in many regions of the pulse. This variation reduced the maximum ejectable area for the system used here and subjected much of the structure to unnecessarily high fluences. We do not know the upper area for the system as described. After a single 5 × 5 mm specimen did not eject, we finished process development and solar cell prototyping using 4 × 4 mm, to conserve the precious epitaxial solar cell material. At a minimum, future experiments should explore flat laser spatial profiles—working near the critical ejection fluence—with sufficient energy and diameter to extend beyond the edges of order 1–100 cm^2 ejection specimens. Such large, flat, and oversized pulses would eliminate many sources

of experimental uncertainty (such as edge effects during processing and multishot ejection) and demonstrate the reliability of splitting crystals by wavelength- and epitaxially selective absorption.

Prior transmission electron microscopy (TEM) and X-ray diffraction work showed that GaAs thin films ejected from a GaAs substrate were free from misfit dislocations and had the same structural quality.[23] We used TEM to search for dislocations and disordering in a laser-ejected, finished GaAs cell (Figures 3D–3F). Using an ejected solar cell from this batch that failed during photovoltaic testing, we removed a cross-sectional lamella from between the front Au contact pad and the rear Au contact using a focused Ga ion beam and micromanipulators (Figure 3A). The transmission electron micrographs revealed the single-crystalline multilayers characteristic of high-performing III-V photovoltaic cells. We found atomically coherent interfaces and no misfit dislocations, a consequence of targeting III-V compositions that are lattice matched to GaAs (and whose composition deviations were not sufficient to exceed critical stresses during growth). These data also show that the crystalline thin films and precise interfaces persisted even though the layers were within about 1 μm of a fast, intracrystalline ablation transient. It is especially notable that both the rear Au contact and the front GaInAsN contact layer were intact after ejection, as these layers would absorb and reflect any energy transmitted during the first few ns of the laser pulse, before the absorber layer became opaque. These data support the conclusion that, for the bonding conditions, specimen design, laser system, and ejection scheme used in this work, the amplitude and duration of the thermomechanical transients during and after ejection do not necessarily damage the finished crystals.

On the substrate side, we have not demonstrated regrowth, even though substrate recovery and regrowth is one key motivation to separate device layers. Dark-field images of the post-ejection substrate clearly show that it is possible to damage the substrate through the 1 μm GaInP etch stop (Note S4; Figure S4C, left). Even with our highly inhomogeneous laser cross-section, single-shot ejection mitigates this damage considerably (Note S4; Figure S4C, right). Independent of improvements to, for example, laser pulse spatial homogeneity, laser pulse duration, and the choice of etch stop alloys, the lower etch stop layer could simply be grown thicker. The process is also particularly amenable to using multiple post-ejection, orthogonal wet etches to restore growth surfaces.[37] We therefore hypothesize that relatively straightforward characterization and process iteration will yield high-quality regrowth without resorting to chemo-mechanical polishing, and that total material loss per ejected area will be of the same order as the thickness melted around the absorber.

Notable technique properties

Our solar cells were removed from their growth substrate with a ~10 ns laser pulse and are the largest single-crystalline devices that we have ejected via pulsed laser energy. Damage was restricted to within approximately 1 μm of a pre-determined epitaxial interface, and the ejected film was only 3.5 μm thick; both of these dimensions are smaller than those we found reported for spalling.[20,21] Crystal ejection is a special case of laser liftoff, but it differs in many ways from, for example, the laser liftoff of GaN from sapphire.[38] Arguably, the most striking differences are that crystal ejection divides a single crystal lattice, that this is possible by virtue of an alloy that is lattice matched to GaAs but has a relatively small band gap, and that other lattice-matched compounds can be grown around the absorber that have large wet-etch selectivities and negligible laser absorption. As we will discuss, the differences

lead to powerful scaling hypotheses for thin film crystal making. We postulate that crystal ejection's processing space has at least seven important dimensions: (1) laser wavelength, (2) pulse duration, (3) pulse energy, (4) laser spatial profile, (5) multilayer architecture (including thicknesses, compositions, and metal reflectors), (6) initial strain (intrinsic, as well as bonding-induced), and (7) surface treatments. Beyond successful ejection of these 4 × 4 mm glass|Ti|Au|III-V structures, we do not know the ultimate ejected-area limit at any point in the processing space, nor the minimum amount of material that must be sacrificed for ejection and device finishing. However, at least for 1–10 ns, 1064 nm, Nd:YAG lasers, wafer-scale pulses can be created at tens of Hz with commercial laser systems (see, for example, https://ekspla.com/products/high-intensity-laser-systems/). Coupled with the present results, and with the accuracy of MOVPE, this suggests that it is already possible to eject lithographically patterned arrays of mm-scale III-V devices, even if thermomechanical cracks or other issues emerge with larger, continuous thin films.

Various facets of this process demonstration motivate discussions about scalability and fundamental crystal creation limits. Our process consists of epitaxy, bonding, laser ejection via free space, and post-ejection finishing. In principle, our post-epitaxial surface never has to touch more than one substance, for example a gold contact. We ejected in air here but could also use an inert atmosphere or even a vacuum. The volume that forms between surfaces during ejection, at least at small displacements or in vacuum, will consist only of excited material from within the crystal. In other words, the ejection process only requires enough empty space for the crystals to separate, and then the new surfaces cool in their own, ultrapure environment. To reveal a pristine interface, we chose to remove the debris and etch stops by rapid wet etching. These layers can be etched away relatively slowly via dilute mixtures, or at 1 to 10 μm per min with standard, room temperature solutions. After removing the melt debris, another short etch reveals the final interface, e.g., the device's surface. But, for nearly all of this time, the etchant is not in contact with the device's front contact surface. No part of the front contact is exposed to the etchant until the final moments of the last etch, during the brief time that it takes to clear uneven etch fronts and verify completion before rinsing. Coupled with the variety of flow, chemistry, temperature, and orientation options available to us by avoiding thick etches and chemical undercutting, it is reasonable to expect that this process can minimize reaction product surface contamination,[16] as well as surface roughness, especially for material-etchant pairs with small etch rate ratios. Hence, assuming that insoluble or otherwise persistent phases are avoidable, this process shows ideal characteristics for generalized III-V crystal splitting, bonding, and etching.

This process may also approach fundamental rate and volumetric processing limits for single-crystalline III-V optoelectronics. Our etch times were independent of device area, and we rapidly etched layers in vertical configurations. We did not peel thin films, use stressor layers, or need any of the concomitant equipment, material, or controls in our process environment. Therefore, we might minimize etch bath volumes, evaporation rates, bath contamination, cleanroom contamination, cleanroom volume, energy consumption, process interruption losses, and waste while maximizing purity, recovery, recyclability, and production rate per volume. Our results suggest pathways to, for example, square-meters-per-second throughput from an order 10 m^2 commercial laser station and ~0.1 m^3 chemical baths, and competing across a variety of interesting fabrication metrics, such as peak watts solar per manufacturing volume per time.

It is remarkable that such a wide, thin, single-crystalline multilayer can be split with one laser pulse, via free space, without stressor layers, and with rigid (or flexible[23]) boundary conditions. Characterizing and understanding the intracrystalline transients is a complex, multidisciplinary problem, especially given the breadth of this processing space. Nevertheless, it is reasonable to guess that our crystals separated along the absorber plane on order 10 ns timescales. This would be an order of magnitude faster than speed-of-sound propagation times across even the modest length scale demonstrated here. Furthermore, we are essentially optically disassembling a (quasi) single-crystal lattice everywhere at once across two dimensions. This implies that ultrafast electron-photon or electron-phonon coupling and local phase transformation times will set the ultimate speed limits for splitting crystals. Finally, because we applied selective optical absorption to split the crystal, we reserved our selective chemical etches for post-separation surface processing. We therefore demonstrated orthogonal processing operations to split crystals and expose interfaces. More generally, we can view wavelength-selective absorption as adding orthogonal dimensions to the traditional III-V processing space and postulate higher-order pathways such as optically guided epitaxial spalling, void-assisted lateral etching, or simply the rapid chemical-mechanical bifurcation of a laser-ejected GaAs|AlAs|GaAs thin film. These processing considerations, and our facile demonstration of single-crystalline minority-carrier devices, imply that crystal ejection could play an important role in the development and proliferation of critical optoelectronics.

EXPERIMENTAL PROCEDURES

Resource availability

Lead contact

Further information and requests for resources should be directed to and will be fulfilled by the lead contact, Bruce M. Clemens (bmc@stanford.edu).

Materials availability

This study did not generate any new unique materials.

Data and code availability

The data and code used during this study are available from the lead author upon reasonable request.

Device fabrication and characterization

Detailed experimental procedures are described in the supplemental experimental procedures.

SUPPLEMENTAL INFORMATION

Supplemental information can be found online at https://doi.org/10.1016/j.xcrp.2023.101449.

ACKNOWLEDGMENTS

B.A.R. was supported by the Department of Defense and Air Force Office of Scientific Research through the National Defense Science & Engineering Graduate Fellowship Program. Part of this work was performed at the Stanford Nano Shared Facilities (SNSF), supported by the National Science Foundation under award ECCS-2026822. B.A.R. thanks Timothy Brand of Stanford's Ginzton Crystal Shop for crystal polishing, NREL's Michelle Young, SLAC's Dr. Mark Welch, Prof. Nick Rolston, and Stanford's Bent and Brongersma Groups for their generous support.

A.M.L. acknowledges support from the Department of Energy, Office of Science, Basic Energy Sciences, Materials Sciences and Engineering Division, under contract DE-AC02-76SF00515. This material is based upon work supported by the US Department of Energy's Office of Energy Efficiency and Renewable Energy (EERE) under the Solar Energy Technologies Office Award Number 34358. The views expressed herein do not necessarily represent the views of the US Department of Energy or the United States Government.

AUTHOR CONTRIBUTIONS

Conceptualization, B.A.R. and B.M.C.; investigation, B.A.R. (laser ejection, cell fabrication, X-ray diffraction [XRD], and photoluminescence [PL]), Z.Z. (TEM), M.A.S. (PV characterization, cell design, and epitaxy), and T.E.C. (evaporation); writing – original draft, B.A.R.; writing – review & editing, all authors; funding acquisition, B.A.R., M.A.S., A.M.L., and B.M.C.; resources, M.A.S. and A.M.L.; supervision, M.A.S., A.M.L., and B.M.C.

DECLARATION OF INTERESTS

B.M.C. has an active patent for crystal ejection, US patent 9,698,053 B2. The patent covers the laser removal of semiconductor thin films by wavelength-selective absorption in relatively low-band-gap, lattice-matched layers.

INCLUSION AND DIVERSITY

We support inclusive, diverse, and equitable conduct of research.

Received: September 23, 2022
Revised: April 7, 2023
Accepted: May 15, 2023
Published: June 6, 2023

REFERENCES

1. Stringfellow, G. (1989). Organometallic Vapor-phase Epitaxy: Theory and Practice (Academic Press Inc.). https://doi.org/10.1016/C2009-0-22261-6.

2. Rumble, J., ed. (2021). Abundance of elements in the earth's crust and sea. In CRC Handbook of Chemistry and Physics, 102nd ed. https://doi.org/10.1201/b17118.

3. Zeng, C., Gonzalez-Alvarez, A., Orenstein, E., Field, J.A., Shadman, F., and Sierra-Alvarez, R. (2017). Ecotoxicity assessment of ionic As(III), As(V), In(III) and Ga(III) species potentially released from novel III-V semiconductor materials. Ecotoxicol. Environ. Saf. *140*, 30–36. https://doi.org/10.1016/j.ecoenv.2017.02.029.

4. Ghandhi, S. (1994). VLSI Fabrication Principles: Silicon and Gallium Arsenide 2ed (John Wiley & Sons).

5. Rudolph, P., and Jurisch, M. (1999). Bulk growth of GaAs, an overview. J. Cryst. Growth *198-199*, 325–335. https://doi.org/10.1016/S0022-0248(98)01208-1.

6. Kayes, B.M., Nie, H., Twist, R., Spruytte, S.G., Reinhardt, F., Kizilyalli, I.C., and Higashi, G.S. (2011). 27.6% Conversion efficiency, a new record for single-junction solar cells under 1 sun illumination. 37th IEEE Phot. Spec. Conf. *4*. https://doi.org/10.1109/PVSC.2011.6185831.

7. Sasaki, K., Agui, T., Nakaido, K., Takahashi, N., Onitsuka, R., and Takamoto, T. (2013). Development of InGaP/GaAs/InGaAs inverted triple junction concentrator solar cells. AIP Conf. Proc. *1556*, 22. https://doi.org/10.1063/1.4822190.

8. Chiu, P.T., Law, D.C., Woo, R.L., Singer, S.B., Bhusari, D., Hong, W.D., Zakaria, A., Boisvert, J., Mesropian, S., King, R.R., and Karam, N.H. (2014). 35.8% space and 38.8% terrestrial 5J direct bonded cells. 40th IEEE Phot. Spec. Conf. *11*. https://doi.org/10.1109/PVSC.2014.6924957.

9. Green, M.A., Dunlop, E.D., Siefer, G., Yoshita, M., Kopidakis, N., Bothe, K., and Hao, X. (2023). Solar cell efficiency tables (Version 61). Progress in Photovoltaics. *31*, 3–16. https://doi.org/10.1002/pip.3646.

10. Horowitz, K.A., Remo, T.W., Smith, B., and Ptak, A.J. (2018). A Techno-Economic Analysis and Cost Reduction Roadmap for III-V Solar Cells. NREL/TP-6A20-72103. https://doi.org/10.2172/1484349.

11. Ward, J.S., Remo, T., Horowitz, K., Woodhouse, M., Sopori, B., VanSant, K., and Basore, P. (2016). Techno-economic analysis of three different substrate removal and reuse strategies for III-V solar cells. Prog. Photovoltaics. *24*, 1284–1292. https://doi.org/10.1002/pip.2776.

12. Hjort, K. (1996). Sacrificial etching of III-V compounds for micromechanical devices. J. Micromech. Microeng. *6*, 370–375. https://doi.org/10.1088/0960-1317/6/4/003.

13. Yablonovitch, E., Gmitter, T., Harbison, J.P., and Bhat, R. (1987). Extreme selectivity in the liftoff of epitaxial GaAs films. Appl. Phys. Lett. *51*, 2222–2224. https://doi.org/10.1063/1.98946.

14. Konagai, M., Sugimoto, M., and Takahashi, K. (1978). High efficiency GaAs thin film solar cells by peeled film technology. J. Cryst. Growth *45*, 277–280. https://doi.org/10.1016/0022-0248(78)90449-9.

15. Yoon, J., Jo, S., Chun, I.S., Jung, I., Kim, H.-S., Meitl, M., Menard, E., Li, X., Coleman, J.J., Paik, U., and Rogers, J.A. (2010). GaAs photovoltaics and optoelectronics using releasable multilayer epitaxial assemblies. Nature *465*, 329–333. https://doi.org/10.1038/nature09054.

16. Cheng, C.-W., Shiu, K.T., Li, N., Han, S.-J., Shi, L., and Sadana, D.K. (2013). Epitaxial lift-off process for gallium arsenide substrate reuse and flexible electronics. Nat. Commun. *4*, 1577. https://doi.org/10.1038/ncomms2583.

17. van Niftrik, A.T.J., Schermer, J.J., Bauhuis, G.J., Mulder, P., Larsen, P.K., and Kelly, J.J. (2007). A diffusion and reaction related model of the epitaxial lift-off process. J. Electrochem. Soc. *154*, D629. https://doi.org/10.1149/1.2779968.

18. Suo, Z., and Hutchinson, J.W. (1989). Steady-state cracking in brittle substrates beneath adherent films. Int. J. Solids Struct. *25*, 1337–1353. https://doi.org/10.1016/0020-7683(89)90096-6.

19. Adachi, S. (1994). GaAs and Related Materials: Bulk Semiconducting and Superlattice Properties (World Scientific).

20. Coll, P.G., Neumann, A., Smith, D., Warren, E., Polly, S., Hubbard, S., Steiner, M.A., and Bertoni, M.I. (2021). Sonic lift-off of GaAs-based solar cells with reduced surface facets. 48th IEEE Phot. Spec. Conf. *2141*. https://doi.org/10.1109/PVSC43889.2021.9518656.

21. Park, H., Won, H., Lim, C., Zhang, Y., Han, W.S., Bae, S.-B., Lee, C.-J., Noh, Y., Lee, J., Lee, J., et al. (2022). Layer-resolved release of epitaxial layers in III-V heterostructure via a buffer-free mechanical separation technique. Sci. Adv. *8*, eabl6406. https://doi.org/10.1126/sciadv.abl6406.

22. Sweet, C.A., Schulte, K.L., Simon, J.D., Steiner, M.A., Jain, N., Young, D.L., Ptak, A.J., and Packard, C.E. (2016). Controlled exfoliation of (100) GaAs-based devices by spalling fracture. Appl. Phys. Lett. *108*, 011906. https://doi.org/10.1063/1.4939661.

23. Hayes, G.J., and Clemens, B.M. (2015). Laser liftoff of gallium arsenide thin films. MRS Commun. *5*, 1–5. https://doi.org/10.1557/mrc.2015.2.

24. Jan, A., Reeves, B.A., van de Burgt, Y., Hayes, G.J., and Clemens, B.M. (2018). Threshold fluence measurement for laser liftoff of inp thin films by selective absorption. Adv. Eng. Mat. *20*, 1700624. https://doi.org/10.1002/adem.201700624.

25. Vurgaftman, I., Meyer, J.R., and Ram-Mohan, L.R. (2001). Band parameters for III-V compound semiconductors and their alloys. J. Appl. Phys. *89*, 5815–5875. https://doi.org/10.1063/1.1368156.

26. Kudrawiec, R. (2007). Alloying of GaN_xAs_{1-x} with InN_xAs_{1-x}: a simple formula for the band gap parametrization of $Ga_{1-y}In_yN_xAs_{1-x}$ alloys. J. Appl. Phys. *101*, 023522. https://doi.org/10.1063/1.2424528.

27. Kurtz, S.R., Olson, J.M., Friedman, D.J., Geisz, J.F., Bertness, K.A., and Kibbler, A.E. (1999). Passivation of interfaces in high-efficiency photovoltaic devices. MRS Proc. *573*, 95. https://doi.org/10.1557/PROC-573-95.

28. Capasso, F. (1987). Band-gap engineering: from physics and materials to new semiconductor devices. Science *235*, 172–176. https://doi.org/10.1126/science.235.4785.172.

29. Friedman, D.J. (2010). Progress and challenges for next-generation high-efficiency multijunction solar cells. Curr. Opin. Solid St. M. *14*, 131–138. https://doi.org/10.1016/j.cossms.2010.07.001.

30. Steiner, M.A., Geisz, J.F., García, I., Friedman, D.J., Duda, A., and Kurtz, S.R. (2013). Optical enhancement of the open-circuit voltage in high quality GaAs solar cells. J. Appl. Phys. *113*, 123109. https://doi.org/10.1063/1.4798267.

31. Adachi, S. (1989). Optical dispersion relations for GaP, GaAs, GaSb, InP, InAs, InSb, $Al_xGa_{1-x}As$, and $In_{1-x}Ga_xAs_yP_{1-y}$. J. Appl. Phys. *66*, 6030–6040. https://doi.org/10.1063/1.343580.

32. Boyd, R. (2008). Nonlinear Optics 3ed (Academic Press). https://dl.acm.org/doi/10.5555/1817101.

33. Krishnamurthy, S., Yu, Z.G., Gonzalez, L.P., and Guha, S. (2011). Temperature- and wavelength-dependent two-photon and free-carrier absorption in GaAs, InP, GaInAs, and InAsP. J. Appl. Phys. *109*, 033102. https://doi.org/10.1063/1.3533775.

34. Ohring, M. (2001). Materials Science of Thin Films: Depositon and Structure 2ed (Academic Press), p. 429. https://doi.org/10.1016/B978-0-12-524975-1.X5000-9.

35. Duda, A., Ward, S., and Young, M. (2012). *Inverted Metamorphic Multijunction (IMM) Cell Processing Instructions* NREL/TP-5200-54049. https://doi.org/10.2172/1036035.

36. Geisz, J.F., Kurtz, S., Wanlass, M.W., Ward, J.S., Duda, A., Friedman, D.J., Olson, J.M., McMahon, W.E., Moriarty, T.E., and Kiehl, J.T. (2007). High-efficiency GaInP/GaAsIn/GaAs triple-junction solar cells grown inverted with a metamorphic bottom junction. Appl. Phys. Lett. *91*, 023502. https://doi.org/10.1063/1.3684555.

37. Lee, K., Zimmerman, J.D., Xiao, X., Sun, K., and Forrest, S.R. (2012). Reuse of GaAs substrates for epitaxial lift-off by employing protection layers. J. Appl. Phys. *111*, 033527. https://doi.org/10.1063/1.2753729.

38. Tavernier, P.R., and Clarke, D.R. (2001). Mechanics of laser-assisted debonding of films. J. Appl. Phys. *89*, 1527. https://doi.org/10.1063/1.1338519.